

Pb doped ZnO nanoparticles for the sorption of Reactive Black 5 textile azo dye

Roua Ben Dassi, Baha Chamam, Jean Pierre Méricq, Marc Heran , Catherine Faur, Lassaad El Mir, Chedly Tizaoui and Ismail Trabelsi

ABSTRACT

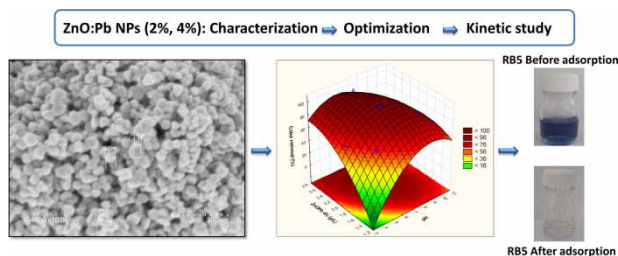
In this study, Pb doped ZnO nanoparticles were synthesized by a sol-gel technique for the sorption of Reactive Black 5 (RB5) textile dye in aqueous solution. The ZnO:Pb (2 and 4%) nanoparticles have been characterized by X-ray diffraction (XRD), Fourier transform infrared spectroscopy, scanning electron microscopy, energy dispersive X-ray spectroscopy and cryogenic nitrogen adsorption method. The average size of the synthesized nanoparticles was less than 100 nm and the surface areas were 18.8 and 20.8 m²/g, respectively for ZnO:Pb 2% and ZnO:Pb 4%. Batch sorption experiments were performed for color removal of RB5 dye at ambient temperature and 30 mg/L dye concentration. The central composite design with response surface methodology was used to study the effect of sorption condition (pH, nanoparticles dose and contact time). The significance of independent variables and their interactions was tested by analysis of variance. The optimum conditions of color removal were pH = 7, 2 g/L dose of nanoparticles and a contact time of 79 min. The color removal performance was 79.4 and 98.1% for ZnO:Pb 2 and 4% respectively. The pseudo-second-order model described well the removal rates while the Langmuir model fitted well the adsorption isotherms.

Key words | color removal, lead doped zinc oxide, nanoparticles, Reactive Black 5, sorption

HIGHLIGHTS

- ZnO:Pb NPs were successful synthesized for the sorption of RB5.
- Central composite design was used to study the effect of operand parameters.
- Pseudo-second-order model described the adsorption data.
- Langmuir monolayer is the best isotherm model.
- A maximum color removal (98.1%) was reached using ZnO:Pb 4%.

GRAPHICAL ABSTRACT



doi: 10.2166/wst.2020.501

Roua Ben Dassi

Baha Chamam

Ismail Trabelsi (corresponding author)

Laboratory of Treatment and Valorization of Water

Reject, CERTE,

Ecopark of Borj-Cedria, 2080 Soliman,

Tunisia

E-mail: ismail.trabelsi@certe.mrt.tn

Roua Ben Dassi

Faculty of Sciences of Bizerte,

University of Carthage,

7021 Jarzouna,

Tunisia

Jean Pierre Méricq

Marc Heran 

Catherine Faur

Institut Européen des Membranes, IEM,

UMR 5635, ENSCM, CNRS, Univ Montpellier,

Montpellier,

France

Lassaad El Mir

Laboratory of Physics of Materials and

Nanomaterials Applied at Environment,

Gabes University,

Faculty of Sciences of Gabes, 6072, Gabes,

Tunisia

Chedly Tizaoui

College of Engineering,

Swansea University,

Bay Campus, Fabian Way, Swansea SA1 8EN,

UK

ABBREVIATIONS

ANOVA	Analysis of variance
BET	Brunauer, Emmett and Teller
CCD	Central composite design
Df	Degrees of freedom
LOF	Lack of fit
MS	Mean square
NPs	Nanoparticles
pH _{pzc}	Point of zero charge
RB5	Reactive Black 5
SS	Sum of squares
TiO ₂ -NPs	Titanium dioxide nanoparticles
ZnO:Fe ₂ O ₃	Iron oxide doped zinc oxide
ZnO:Pb	Lead doped zinc oxide nanoparticles
ZnO:V ₃ %	Vanadium doped zinc oxide

INTRODUCTION

Rapid industrialization has a detrimental effect on the environment with water pollution becoming a major societal problem due to its effects on the ecosystem (Santhosh *et al.* 2016). The textile industry is a major polluter because of the large volumes of heavily contaminated wastewater that it rejects to the environment (Holkar *et al.* 2016). The composition of the textile effluent is a complex mixture of hazardous chemical compounds including unfixed dyes, acids, alkalis, hydrogen peroxide, starch, surfactant, dispersing agents, and metals. Despite being toxic to the aquatic and non-aquatic organisms and that they can cause cancer in humans, azo dyes are the most used dyes (around 70% of all dyes) (Salehi *et al.* 2016). Azo dyes (-N=N-) have complex aromatic molecular structures that resist biodegradation making them persist for long times in the environment (Heibati *et al.* 2014). The direct discharge of textile effluent into the aquatic environment, thus, poses environmental and health problems (Gita *et al.* 2017). Several techniques have been studied for the removal of azo dyes including coagulation–flocculation (Verma *et al.* 2012; Dassi *et al.* 2017), advanced oxidation (Wong *et al.* 2015) and membrane filtration (Riera-Torres *et al.* 2010). Despite showing promising results, these methods have certain defects such as sludge production, high treatment costs and membrane fouling (Crini & Lichtfouse 2019). Adsorption has also been widely studied for dye removal and it appears to be an economical, ecological and

sustainable technique for dye removal (Kumar *et al.* 2013). Many materials show a high adsorption efficiency of textile dyes, such as activated carbon (Singh *et al.* 2003), chitosan (Monvisade & Siriphannon 2009) and geopolymer (Maleki *et al.* 2018). Recently, nanotechnology has been successfully integrated in adsorption processes (nanoadsorbent), membrane processes (membrane composite) and photocatalysis (Qu *et al.* 2013). The sorption using metal oxide nanoparticles (ZnO, Fe₂O₃, TiO₂) has been widely studied, as one of the most advanced materials used for the textile wastewater treatment (Gehrke *et al.* 2015). Zinc oxide (ZnO) nanoparticles (NPs) have been used as advanced adsorption materials in the wastewater treatment (Zhang *et al.* 2016) due to their specific properties such as the presence of active sites at the surface, chemical stability with high efficiency, low cost and low toxicity (Khezami *et al.* 2017a). It was reported that the incorporation of metals such as Fe, Pb, Ni, Cu, Ag and Al in zinc oxide NPs enhances the adsorption capacity and the photocatalytic activity (Bordbar *et al.* 2018; Ebrahimi *et al.* 2019). Farrokhi *et al.* (2014) showed the ZnO–Fe₃O₄ NPs exhibit an efficient removal of azo dye Reactive Black 5 (RB5) with maximum sorption capacity of 22.1 mg/L. Lei *et al.* (2017) reported that ZnO–Al₂O₃ was an efficient adsorbent for the removal of Congo red dye. In this study, novel lead doped zinc oxide NPs were successfully synthesized by the sol-gel technique to remove an anionic textile dye (RB5) from aqueous solution using a batch sorption system. A central composite (CCD) design with response surface methodology was used to understand the interaction between the most influencing parameters (pH, the dose of NPs and contact time) in the sorption and to determine the optimal conditions of the process. Kinetic and isotherm models were used to study the sorption mechanism of RB5 on ZnO:Pb NPs.

MATERIALS AND METHODS

Chemicals

RB5 azo dye in powder form at purity of ≥50% was purchased from Sigma Aldrich, USA (molecular formula C₂₆H₂₁N₅Na₄O₁₉S₆, molecular weight = 991.82 g/mol). Zinc acetate dehydrate (Zn(CH₃COO)₂·2H₂O) 99.99% was used as a zinc precursor, lead(II) nitrate (N₂O₆Pb) 99.99% as doping element source, methanol and ethyl alcohol (EtOH) as solvent and co-solvent respectively, and

sodium hydroxide (NaOH) and hydrochloric acid (HCl) as pH adjustment solutions. All products were purchased from Sigma Aldrich, Germany and used as-received without further purification.

Preparation of hybrid adsorbent ZnO:Pb

Lead-doped ZnO nanocrystals (ZnO:Pb) were prepared using sol-gel method following a method presented in literature (El Mir et al. 2008). Briefly, 16 g of precursor zinc acetate dehydrate was added to 112 mL of methanol and stirred at room temperature for 15 min using a magnetic stirrer. Adequate quantities of lead precursor (0.496 and 0.971 g), corresponding to 2 and 4% atomic percent calculated relative to the sum of atomic masses of Zn and Pb ($[Pb]/([Zn] + [Pb])$), were added to the solution, which was stirred for another 15 min. The solution was then placed in an autoclave (250 °C) and dried under supercritical conditions of EtOH.

Nanoparticles characterization

The ZnO:Pb NPs were characterized with Fourier transform infrared spectroscopy (FTIR) (PerkinElmer, USA) in order to identify the main functional groups present on their surface. The spectral resolution of the FTIR is 1 cm^{-1} measured between 4,000 and 400 cm^{-1} . X-ray diffraction (XRD) pattern was recorded with a Bruker D8 Advance X-ray diffractometer using Cu $K\alpha$ ($\lambda = 1.541 \text{ \AA}$) radiation in the diffraction angle range of 10–100°. The surface morphology of ZnO:Pb nanopowders was characterized by field emission scanning electron microscopy (FE-SEM, Hitachi, S-4800, Japan). Energy dispersive X-ray (EDX, Zeiss EVO HD15) technique was also used to characterize the elemental composition of the adsorbent. The BET (Brunauer–Emmett–Teller) specific surface area, pore volume (micropore volume and total pore volume) and pore size distribution of the nanopowders were determined by nitrogen N_2 adsorption/desorption isotherm at 77 K (Micromeritics, ASAP-2020).

The pH of point of zero charge (pH_{pzc}) of ZnO:Pb (2 and 4%) was measured by the pH drift method (Mustafa et al. 2013). A 5 mM NaCl solution was prepared and its pH was adjusted by adding HCl or NaOH to be in the range 2–12. An amount of 20 mg of ZnO:Pb 2% or 4% was added to 20 mL of the NaCl solution at an initial pH_i in an Erlenmeyer flask stirred at 250 rpm at room temperature for 24 h (Kulkarni et al. 2016). The final pH (pH_f) was

measured and a plot of pH_f vs pH_i was made. The point at which the curve crosses the line $\text{pH}_f = \text{pH}_i$ is the pH_{pzc} .

Experimental design and optimization

A 2^3 factorial design was used to efficiently evaluate the effect of experimental variables on the sorption process and improve performance while minimizing the error of experiments. The 2^3 design is associated with a second-order polynomial model and is composed of eight trials completed by six replicates of the central point and six axial points which are located at α distance from center and make the design rotatable ($\alpha = 1.68$). In this study, the analyzed response variable was the color removal yield (Y); and the three independent variables were pH (X_1), dose of sorbent (X_2) and contact time (X_3). The actual values of the independent variables and their corresponding coded values ($-\alpha, -1, 0, +1, +\alpha$) are presented in Table 1. Experiments were performed in a random order (Table 1) and the optimized conditions were determined using quadratic response surfaces given by a second-order polynomial model (Equation (1)) (Ghaedi et al. 2016):

$$Y = \beta_0 + \sum_{i=1}^n \beta_i X_i + \sum_{i=1}^n \beta_{ii} X_i^2 + \sum_{i=1}^n \sum_{j=1}^n \beta_{ij} X_i X_j \quad (1)$$

where β_0 is the constant term, β_i are the linear coefficients, β_{ii} are the quadratic coefficients and β_{ij} are the interactive coefficients.

The analysis of variance (ANOVA) and the statistical analysis of the effect of individual linear, quadratic and interaction terms on the response were performed using STATISTICA 10 software. The significance of all terms in the polynomial model was assessed statistically by computing the F -value and the P -value at a probability level of 0.05.

Table 1 | Experimental factors and levels in the central composite design

Independent variables	Levels ($\alpha = 1.68$)				
	$-\alpha$	-1	0	$+1$	$+\alpha$
X_1 : pH	3.64	5	7	9	10.36
X_2 : Dose of NPs (g/L)	1.32	1.6	2	2.4	2.67
X_3 : Time (min)	9.60	30	60	90	110.40

Sorption experiments

The dye initial concentration was fixed at 30 mg/L and was prepared by dilution of 1 g/L solution in distilled water. Vials of 5 mL were used for the sorption experiments. The pH was adjusted in the range 3.64–10.36 by the addition of HCl (0.01 M) or NaOH (0.01 M) and measured by a pH meter (Consort C831). A given mass of the adsorbent to achieve a set dose (1.32–2.67 g/L) was added to the flasks, which were then placed in a shaker (Stuart orbital shaker, <http://www.stuart-equipment.com/product.asp?dsl=77>, USA) with a speed of 250 rpm at ambient temperature. At the end of the experiment, the adsorbent was separated from the solution by centrifugation (Sigma 3-16 K, 4,000 rpm for 10 min). The absorbance of RB5 in solution was determined by absorption at $\lambda_{\max} = 597$ nm by a UV-visible spectrophotometer (Shimadzu, UV 2401PC). The efficiency of color removal of RB5 was determined using Equation (2):

$$\text{Color removal (\%)} = \frac{\text{Abs}_i - \text{Abs}_f}{\text{Abs}_i} \times 100 \quad (2)$$

where Abs_i and Abs_f are respectively the initial and final measured absorbance values. For kinetics sorption experiments, 10 mg of ZnO:Pb NPs was added to 5 mL of the 30 mg/L RB5 solution at an initial pH 7 and ambient temperature $20 \pm 2^\circ\text{C}$. Sampling was carried out at different time intervals. Isotherm studies were conducted at a constant mass of ZnO:Pb (10 mg in 5 mL) and varying initial concentrations of the RB5 solution in the range of 20–80 mg/L. The solutions were stirred at ambient temperature $20 \pm 2^\circ\text{C}$ for 24 h. It was verified from the kinetics experiments that 24 h was largely sufficient to reach equilibrium. The adsorption capacity was calculated from mass balance given in Equation (3):

$$Q_{ads} = \frac{(C_o - C_e) \times V}{m} \quad (3)$$

where C_o (mg/L) is the initial concentration, C_e (mg/L) is the dye concentration at equilibrium, Q_{ads} (mg/g) is the amount of dye adsorbed per unit of adsorbent at equilibrium, V (L) is the volume of dye solution and m (g) is the mass of adsorbent.

RESULTS AND DISCUSSION

Characterization of ZnO:Pb

FTIR spectra of Pb doped ZnO NPs are shown in Figure 1(a). It depicts a sequence of absorption bands in the range of 500 and $4,000\text{ cm}^{-1}$. The absorption peaks at 852, 684 and 592 cm^{-1} revealed the presence of Pb-O stretching vibration (Borhade et al. 2013; Sathya & Pushpanathan 2018). The two peaks of absorption, 1,400 and $1,581\text{ cm}^{-1}$, could be attributed to precursor functional groups and ZnO surface-related reaction by-products (Kataria & Garg 2017). The stretching vibration peak of the C-H bond was observed at $3,093\text{ cm}^{-1}$ (Mousavi et al. 2015).

Figure 1(b) depicts the XRD diffractogram of ZnO:Pb nanopowder. The diffraction peaks at $2\theta = 31.75^\circ, 34.23^\circ, 36.05^\circ, 47.39^\circ, 56.35^\circ, 62.65^\circ, 67.80^\circ, 68.2^\circ$ and 69.4° which can be attributed to the (100), (002), (101), (102),

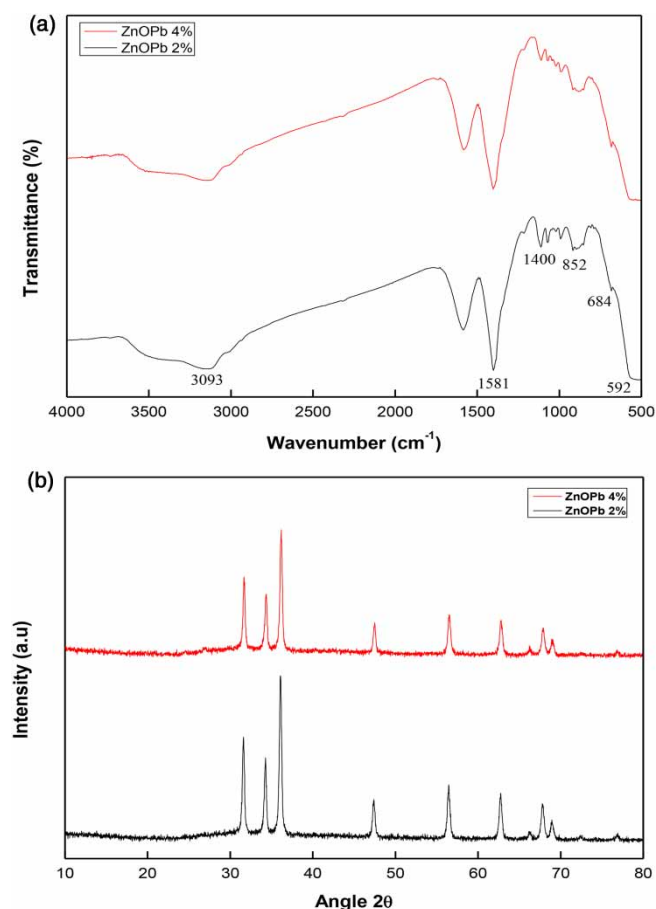


Figure 1 | (a) FTIR analysis of ZnO:Pb nanopowder and (b) XRD pattern of the prepared ZnO:Pb nanopowder.

(110), (103), (200), (112) and (201) planes correspond to ZnO hexagonal wurtzite structure, in agreement with the JCPDS card No. 36-1451 (Kataria & Garg 2017). No characteristic peaks related to Pb metal can be detected, which indicates the successful incorporation of Pb in the ZnO.

The SEM images illustrated in Figure 2(a) and 2(c) exhibited spherical particles with average particle size less than 100 nm. The EDX result (Figure 2(b) and 2(d)) of NPs indicated the existence of 65.7% of zinc and 2.2% of lead for ZnO:Pb 2% and 63.6% of zinc and 4.3% of lead for ZnO:Pb 4%, which confirms the theoretical calculation of NPs composition. The surface area and the pore volume of the ZnO:Pb 2 and 4% were investigated using nitrogen gas adsorption–desorption method based on BET theory. The doping of ZnO by Pb has an influence on the specific surface area of the nanopowder. The total pore volume was found to be 0.177 cm³/g and 0.197 cm³/g respectively for ZnO:Pb 2% and ZnO:Pb 4%. The average

of pore width was 145 and 123 Å for ZnO:Pb 2% and ZnO:Pb 4% respectively.

The incorporation of Pb in zinc oxide NPs increases the specific surface area to 18.8 m²/g for ZnO:Pb 2% and 20.8 m²/g for ZnO:Pb 4%, which are higher than other NPs like ZnO, ZnO:Fe₂O₃ and ZnO:V₃O₅ whose BET surface area ranged from 4 to 9 m²/g (Table 2).

Table 2 | Comparison of BET surface area (S_{BET}) for different NPs

Nanoparticle	S_{BET} (m ² /g)	Reference
ZnO	8.25	Khezami <i>et al.</i> (2017a)
ZnO:Fe ₂ O ₃	4.51	Khezami <i>et al.</i> (2017b)
ZnO:V ₃ O ₅	8.10	Khezami <i>et al.</i> (2016)
ZnO:Pb 2%	18.8	Present study
ZnO:Pb 4%	20.8	Present study

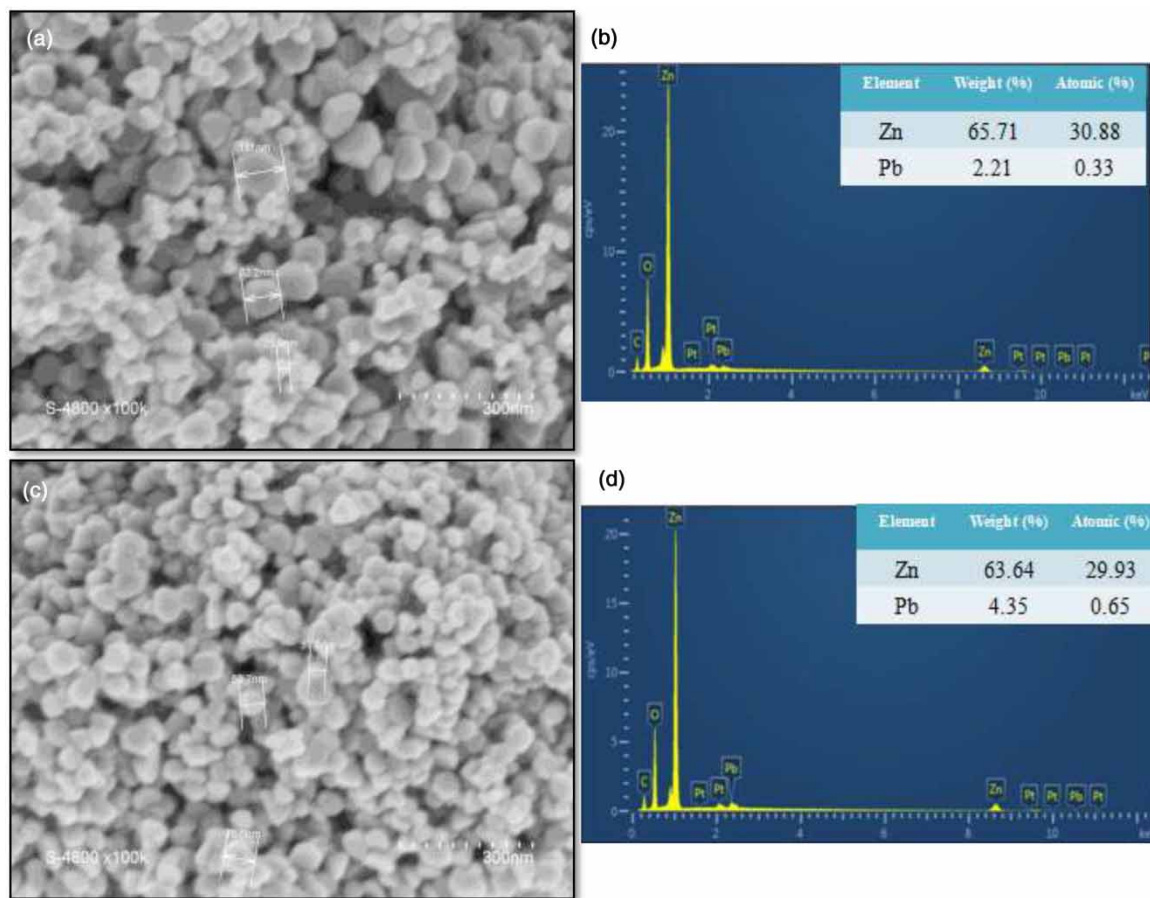


Figure 2 | SEM images and EDX analysis of ZnO:Pb 2% (a and b) and ZnO:Pb 4% (c and d).

The point of zero charge

Figure 3 presents the pH_{pzc} of ZnO:Pb 2% and ZnO:Pb 4% NPs. The figure shows that both ZnO:Pb 2 and 4% have the same pH_{pzc} value of 7.5. At pH less than pH_{pzc} , the surface of the ZnO:Pb NPs is positively charged and, due to electrostatic interactions, the adsorption of the anionic dye is thus preferred (Farrokhi et al. 2014). However, when the pH is greater than pH_{pzc} , the surface of the NPs is negatively charged and, due to electrostatic repulsion forces, the adsorption efficiency of RB5 decreases (Samadi et al. 2015).

Analysis of central composite design

The central composite design was used to estimate the influence of three factors: pH, dose of NPs and contact time in the range of pH 3.6–10.3, NPs dose (g/L) 1.32–2.67 and contact time (min) 46.4–113.6. The experimental and predicted removals (%) of RB5 for the 20 experiments are presented in Table 3.

The ANOVA presented in Table 4, gives useful information about the significance of the variables and their interaction based on F and P values at 95% confidence level. The significance of the model terms was investigated by P -value. A P -value less than 0.05 in the ANOVA table indicates that the interactions between the significant factors have a good influence on the response. Lack of fit (LOF) compares the experimental error of the replicate measurements. The non-significance (F -value >0.05) of lack of fit indicate the model was appropriate to predict the adsorption percentage within the investigated range of variables (Dil et al. 2019). The F -value of LOF for the present

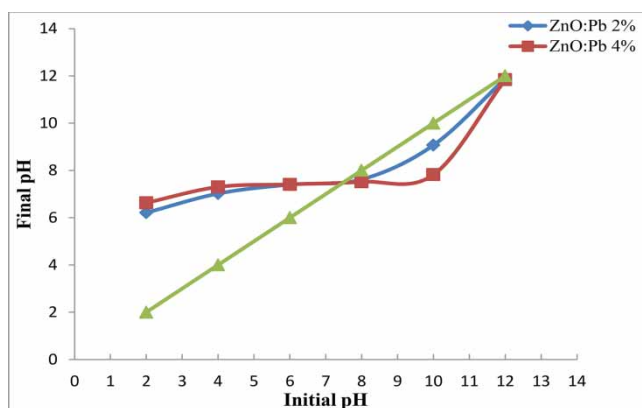


Figure 3 | Determination of the pH_{pzc} of ZnO:Pb 2% and ZnO:Pb 4% NPs.

study (Table 4) indicates a good concordance between the experimental and the predicted RB5 removal efficiencies. The high values of the correlation coefficients ($R^2 = 0.97$ for ZnO:Pb 2% and $R^2 = 0.95$ for ZnO:Pb 4%) show a high significance of the model.

The model-predicted values as a function of the observed values for ZnO:Pb 2% and ZnO:Pb 4% are presented respectively in Figure 4(a) and 4(b) (circles) as well as the corresponding regression plots (lines). A positive regression coefficient means that an increase in the factor value leads to an increase in the response value (a synergistic effect). In the opposite case when the regression coefficient is negative, an increase in the variable value results in a decrease of the response value (an antagonistic effect). The analysis of the experimental results allowed the determination of the coefficients of the quadratic response second-order polynomial model for both ZnO:Pb 2 and 4% (Equations (4) and (5)):

$$Y_1(\text{ZnO:Pb } 2\%) = 77.60 - 10.10X_1 - 12.21X_1^2 + 24.20X_2 - 8.56X_2^2 + 7.58X_3 + 6.32X_1X_3 - 10.07X_2X_3 \quad (4)$$

$$Y_2(\text{ZnO:Pb } 4\%) = 98.13 + 7.57X_1 + 21.41X_1^2 + 17.33X_2 - 12.91X_2^2 + 5.91X_3 - 4.11X_3^2 - 15.95X_1X_2 + 3.67X_1X_3 - 4.11X_2X_3 \quad (5)$$

Equations (4) and (5) emphasize the interaction effect of the factors on the removal of RB5 by ZnO:Pb 2% and ZnO:Pb 4%. A positive impact of a factor means an improvement in the response when the factor level increases, while a negative impact means that the response is not improved with increasing the factor levels.

Response surface methodology

The three-dimensional response surface plots (Figure 5) show the interaction effect of the three variables, pH, dose of NPs and contact time, on the efficiency removal (%) of RB5. The pH of the solution is an important parameter during the dye sorption process. The effect of pH on the removal of RB5 was examined between pH 3.6 and 10.3 (Figure 5(a), 5(d), 5(c) and 5(f)). RB5 is an anionic dye, which exists in the aqueous solution in the form of negatively charged ions. As a charged species, the adsorption degree on the surface of the adsorbent is mainly influenced by the surface charge of the adsorbent, which in turn is

Table 3 | Data statistics of model variables

Runs	Independent factors			% Color removal ZnO:Pb 2%			% Color removal ZnO:Pb 4%		
	pH	Dose of NPs (g/L)	Contact time (min)	Observed	Predicted	Residual	Observed	Predicted	Residual
1	5	1.6	30	59.27	58.59	0.67	63.37	58.93	4.44
2	9	1.6	30	38.44	41.09	-2.64	80.54	77.17	3.36
3	5	2.4	30	83.06	87.43	-4.37	91.62	93.30	-1.68
4	9	2.4	30	74.19	74.90	-0.70	84.45	82.22	2.23
5	5	1.6	90	68.81	68.96	-0.14	64.32	64.76	-0.44
6	9	1.6	90	66.53	63.01	3.51	93.24	89.76	3.47
7	5	2.4	90	81.18	79.38	1.79	90.00	91.57	-1.57
8	9	2.4	90	76.88	78.41	-1.53	8.59	87.24	-2.65
9	3.6	2	60	72.04	71.25	0.79	64.32	63.93	0.38
10	10.3	2	60	57.12	56.71	0.41	74.18	77.23	-0.04
11	7	1.32	60	48.65	49.90	-1.24	62.56	68.16	-5.59
12	7	2.67	60	89.51	87.06	2.45	97.97	94.92	3.05
13	7	2	9.6	72.71	70.71	2.00	82.29	88.38	-6.09
14	7	2	110.4	80.24	82.36	-2.12	99.59	97.51	2.07
15	7	2	60	78.49	79.53	-1.03	97.56	98.28	-0.72
16	7	2	60	77.95	79.53	-1.57	97.83	98.28	-0.45
17	7	2	60	79.83	79.53	0.30	97.70	98.28	-0.58
18	7	2	60	79.56	79.53	0.03	98.24	98.28	-0.04
19	7	2	60	79.16	79.53	-0.36	97.97	98.28	-0.31
20	7	2	60	78.76	75.00	3.75	97.83	93.68	4.15

Table 4 | ANOVA for CCD of ZnO:Pb 2% and ZnO:Pb 4%

Source of variation	ZnO:Pb 2%					ZnO:Pb 4%				
	SS	df	MS	F-value	P-value	SS	df	MS	F-value	P-value
X ₁	347.468	1	347.468	483.943	0.000025	194.877	1	194.877	2,435.43	0.000001
X ₁ ²	522.755	1	522.755	728.079	0.000011	1,606.743	1	1,606.743	20,079.95	0.000000
X ₂	1,997.827	1	1,997.827	2,782.516	0.000001	1,024.944	1	1,024.944	12,809.02	0.000000
X ₂ ²	259.436	1	259.436	361.335	0.000045	589.434	1	589.434	7,366.33	0.000000
X ₃	209.175	1	209.175	291.332	0.000069	126.924	1	126.924	1,586.20	0.000002
X ₃ ²	18.323	1	18.323	25.520	0.007222	57.619	1	57.619	720.08	0.000011
X ₁ X ₂	14.803	1	14.803	20.617	0.010492	509.180	1	509.180	6,363.38	0.000000
X ₁ X ₃	79.974	1	79.974	111.386	0.000456	27.033	1	27.033	337.84	0.000052
X ₂ X ₃	202.952	1	202.952	282.666	0.000073	33.910	1	33.910	423.78	0.000033
Lack of fit	92.748	6	15.458	21.529	0.005198	201.837	6	33.640	420.40	0.000015
Pure error	2.872	4	0.718			0.320	4	0.080		
Total SS	3,589.247	19				4,097.946	19			

influenced by the pH of the solution (Bazrafshan *et al.* 2015). According to the results of pH_{pzc} of ZnO:Pb 2% and ZnO:Pb 4% NPs, at pH below the pH_{pzc} (7.5) of the adsorbent

the surface of the sorbent is positively charged and able to attract the negatively charged dye molecule from the solution. Electrostatic attraction exists between the positively

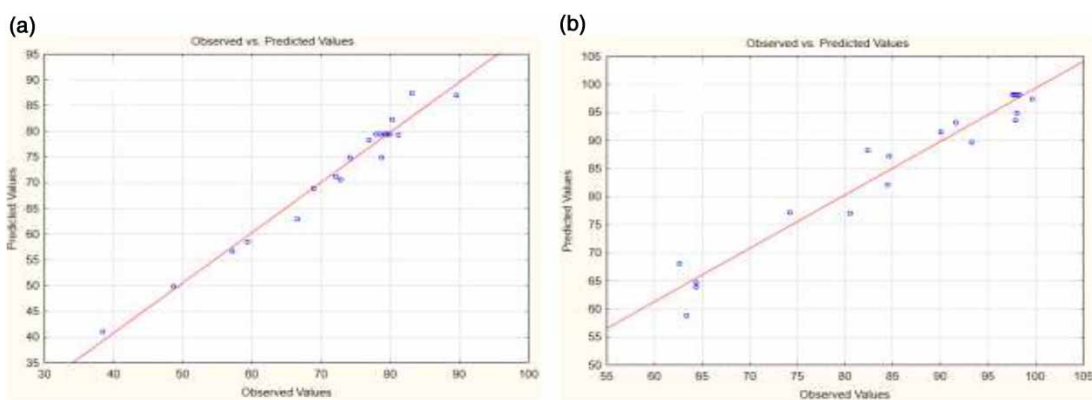


Figure 4 | Plot of the measured and model predicted values of the response variable (a): ZnO:Pb 2%; (b): ZnO:Pb 4%.

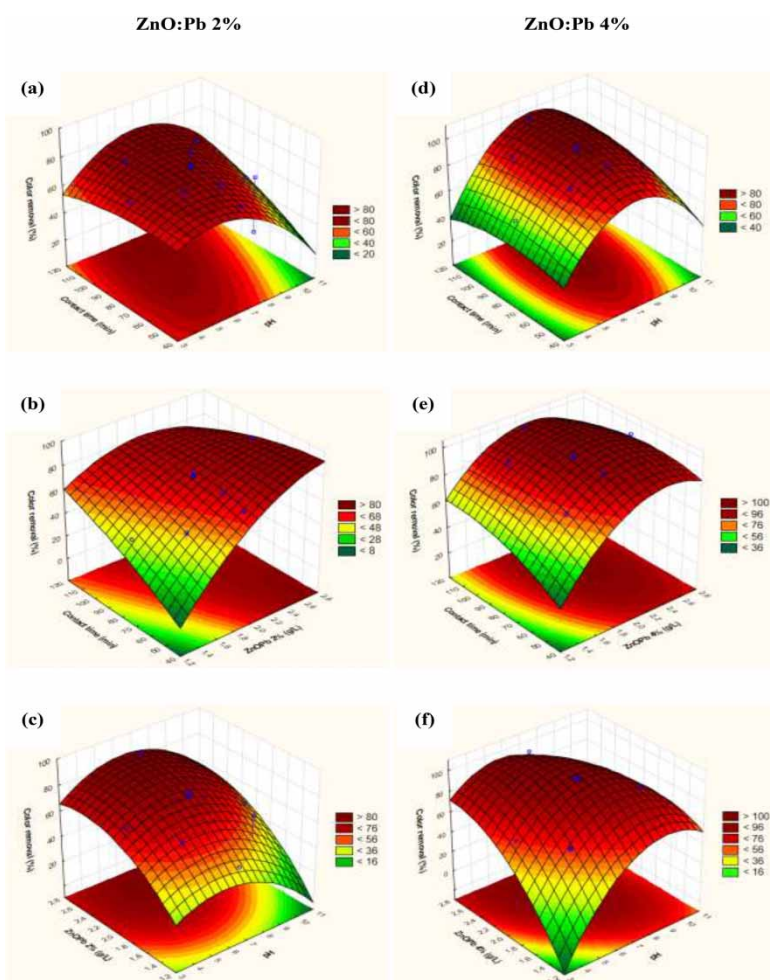


Figure 5 | 3D response surface plot of color removal of RB5 as the function of: (a and d) pH and contact time (NPs dose = 2 g/L); (b and e) NPs dose and contact time (pH = 7); (c and f) pH and NPs dose (contact time = 79 min). Initial dye concentration of 30 mg/L.

charged surface of the adsorbent and the negative charge of the RB5 textile dye (due to the presence of $-\text{SO}_3^-$ groups). The maximum removal efficiency of RB5 was observed at

neutral pH for both of the NPs. The highest RB5 removal efficiencies (more than 80%) were observed when increasing the contact times and the dose of NPs simultaneously

(Figure 5(b) and 5(e)). As expected, the dye removal percentage increased when the dose of adsorbent increased. This can be explained by the increase of active sites on the surface of the nanoadsorbent. Similar results were observed in the literature for the removal of RB5 by ZnO-Fe₂O₃ NPs (Farrokhi *et al.* 2014) and RB5 by iron oxide NPs (Chang & Shih 2018). The optimal conditions of color removal using ZnO:Pb 2% and ZnO:Pb 4% NPs were pH 7, adsorbent dose 2 g/L and contact time of 79 min with maximum color removal of 79.4 and 98.1% respectively.

Desirability function

The maximum color removal efficiency for RB5 dye by ZnO:Pb 2% and ZnO:Pb 4% corresponding to the optimal experimental conditions of the independent variables were determined by using the desirability function on the STATISTICA 10.0.0 software (Table 5). The optimum conditions were found by the model to be pH 7, amount of NPs 2 g/L and time 79 min, giving an experimental maximum RB5 removal of 79.4 and 98.1% for ZnO:Pb 2% and ZnO:Pb 4% respectively. In order to confirm the model adequacy, confirmatory experiments were conducted with these optimal parameters. Results gave a percentage RB5 removal of 80.6 and 97.1% for ZnO:Pb 2% and ZnO:Pb 4%. The percentage error difference between the experimental and predicted value was low (<1.5%) which validated the findings of response surface optimization and indicates that the proposed model is adequate for obtaining the optimum value in the range of the studied parameters.

Kinetic study

The rate of dye adsorption was determined using pseudo-first order, pseudo-second-order and intra-particle diffusion kinetic models. These models are expressed, respectively,

in linear forms by Equations (6)–(8):

$$\log(q_e - q_t) = \log q_e - \left(\frac{K_1}{2.303} \right) t \quad (6)$$

$$\frac{t}{q_t} = \frac{1}{K_2 q_e^2} + \frac{t}{q_e} \quad (7)$$

$$q_t = K_{id} t^{1/2} + C \quad (8)$$

where q_e and q_t (mg/g) are the adsorption capacities at equilibrium time and at time t , respectively, K_1 (1/min) is the kinetic rate constant, K_2 (g/mg/min) is the pseudo-second-order rate constant, K_{id} (mg/g/min^{1/2}) is the intra-particle diffusion rate constant and C is the intra-particle diffusion constant.

The effect of contact time on color removal was studied at pH = 7 using 30 mg/L of RB5, shown in Figure (6). The result shows that at 15 min of contact time the color removal percentage was 65.2 and 65.9% for ZnO:Pb 2 and 4% respectively. The sorption process was fast and after 90 min of contact time ZnO:Pb 2 and 4% achieved 79 and 98% maximum percentage removal of the dye respectively.

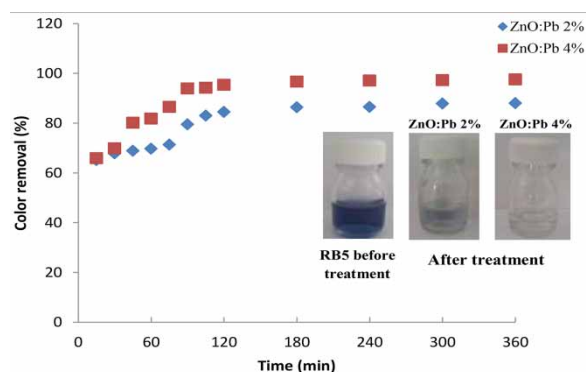


Figure 6 | Effect of contact time on color removal at pH = 7, [RB5] = 30 mg/L and T = 20 ± 2 °C.

Table 5 | Validation of optimized conditions for RB5 dye adsorption on ZnO:Pb 2% and ZnO:Pb 4%

Variables	Optimum value	Responses				Desirability	
		Observed		Predicted		ZnO:Pb 2%	ZnO:Pb 4%
		ZnO:Pb 2%	ZnO:Pb 4%	ZnO:Pb 2%	ZnO:Pb 4%		
pH	7	79.4	98.1	80.6	97.1	0.80	0.96
NPs dose (g/L)	2						
Time (min)	79						

The experimental data were fitted by the pseudo-first-order, pseudo-second-order and intra-particle diffusion models plotted in Figure (7) and the values of the models' rate constants are given in Table 6. The pseudo-second-order model showed excellent fit of the adsorption data for both adsorbents with R^2 values of 0.998 and 0.999 for ZnO:Pb 2% and ZnO:Pb 4% respectively. The pseudo-second-order model makes it possible to characterize the adsorption of RB5 onto ZnO:Pb NPs.

Isotherm study

Langmuir, Freundlich and Dubinin–Radushkevich isotherm models were examined to describe adsorption equilibrium and to study the interaction between adsorbent and adsorbate species and adsorption capacity of adsorbent.

The Langmuir isotherm supports monolayer coverage of adsorbate without interaction between adsorbed molecules. The linearized equation for the Langmuir isotherm can be

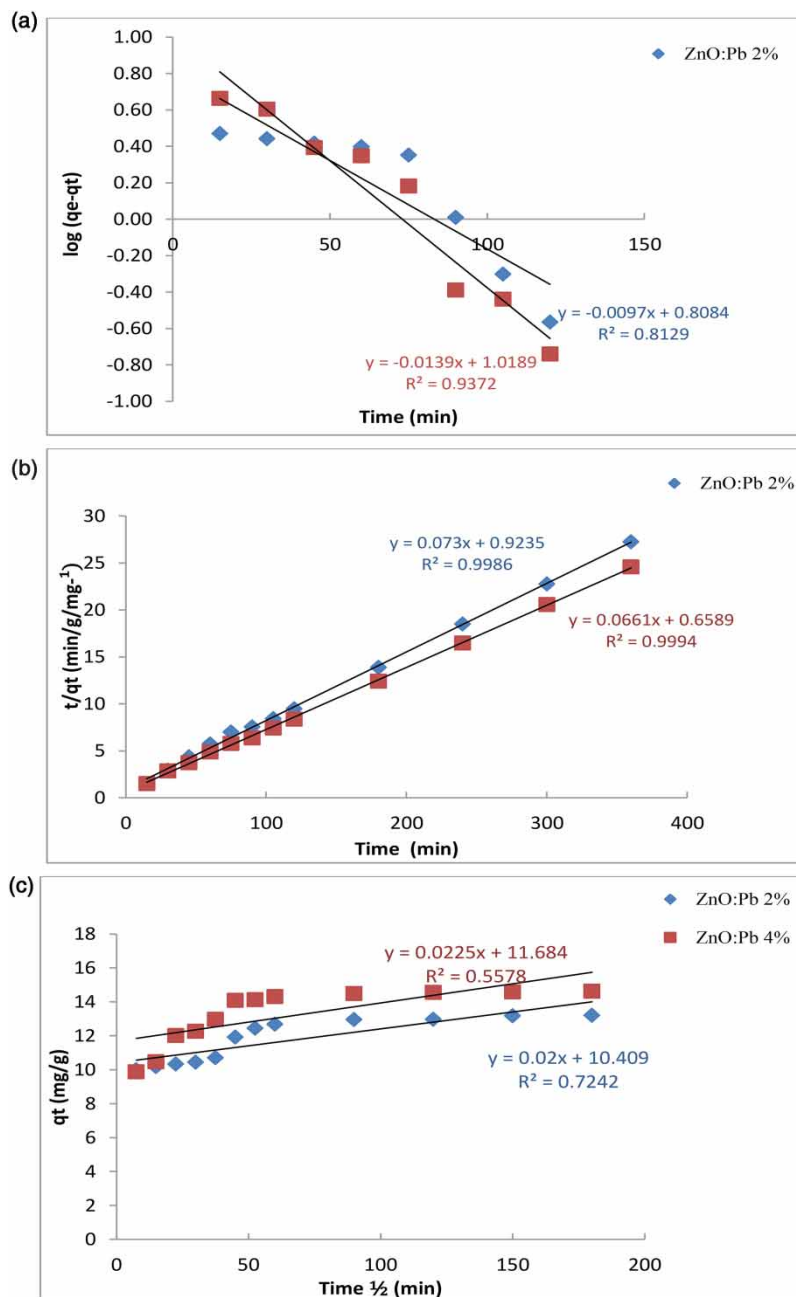


Figure 7 | (a) Pseudo-first-order, (b) pseudo-second-order and (c) intra-particle diffusion models for RB5 adsorption onto ZnO:Pb NPs.

Table 6 | Kinetic parameters of RB5 removal using ZnO:Pb 2% and ZnO:Pb 4%

Kinetic model	Plot	Parameter	[RB5] = 30 mg/L	
			ZnO:Pb 2%	ZnO:Pb 4%
First-order	Log ($q_e - q_t$) vs t	q_e (mg/g)	7.29	10.44
		K_1 (1/min)	0.018	0.032
		R^2	0.812	0.937
Second-order	t/q_t vs t	q_e (mg/g)	13.69	15.12
		K_2 (g/mg/min)	0.28	0.31
		R^2	0.998	0.999
Intra-particle diffusion	q_t vs $(t)^{1/2}$	K_{id} (mg/g/min ^{1/2})	0.02	0.22
		C (mg/g)	10.4	11.68
		R^2	0.724	0.557

expressed by Equation (9) (Langmuir 1916):

$$\frac{C_e}{q_e} = \frac{1}{K_L q_m} + \frac{C_e}{q_m} \quad (9)$$

where C_e is the equilibrium concentration of dye in the solution (mg/L), q_e is the equilibrium capacity of dye on the adsorbent (mg/g), q_m is the maximum adsorption capacity of the adsorbent corresponding to the complete monolayer coverage on the surface (mg/g), and K_L is the Langmuir adsorption constant (L/mg). The data of the Langmuir isotherm were obtained by the plot of C_e/q_e versus C_e as in Figure 8(a). The essential characteristic of the Langmuir isotherm can be expressed by a dimensionless separation factor called the equilibrium parameter R_L given by Equation (10):

$$R_L = \frac{1}{1 + K_L C_e} \quad (10)$$

R_L value indicates the adsorption nature as irreversible if $R_L = 0$, favorable if $0 < R_L < 1$, linear if $R_L = 1$ and unfavorable if $R_L > 1$.

The Freundlich empirical model assumes heterogeneity of the adsorbent surface which appears to be due to different functional groups on surface sites. The linear form of the Freundlich isotherm can be expressed by Equation (11) as follows (Freundlich 1906):

$$\log q_e = \log K_f + \frac{1}{n} \log C_e \quad (11)$$

where K_f and $1/n$ are characteristic constants representing the adsorption capacity and the adsorption intensity of the system respectively; the values of K_f and $1/n$ are obtained from the linear plot of $\log q_e$ versus $\log C_e$. The data of the

Freundlich isotherm were obtained by the plot of $\log q_e$ versus $\log C_e$ as in Figure 8(b).

The Dubinin–Radushkevich isotherm model was applied to estimate the porosity, free energy and the characteristics of adsorbents (Dubinin 1947). The Dubinin–Radushkevich isotherm is applicable to homogeneous surfaces. Constant adsorption potential is calculated from the linear Equation (12) (Montazer-Rahmati et al. 2011):

$$\ln q_e = \ln q_s - K \epsilon^2 \quad (12)$$

where q_s is the theoretical saturation capacity (mg/g), K is a constant related to mean free energy of adsorption per mole of the adsorbate (mol^2/J^2) and ϵ is the Polanyi potential which is related to equilibrium as the Equation (13) shows:

$$\epsilon = RT \ln(1 + 1/C_e) \quad (13)$$

The data of the Dubinin–Radushkevich isotherm were obtained by the plot of $\log q_e$ versus ϵ^2 as in Figure 8(c). Dubinin–Radushkevich isotherm parameters K and q_s were determined by linear regression, and R^2 values are listed in Table 7.

Table 7 summarizes the Langmuir, Freundlich and Dubinin–Radushkevich isotherm constant parameters and the correlation coefficients calculated for the sorption of RB5 onto ZnO:Pb 2 and 4%. The determination coefficients (R^2) for Langmuir, Freundlich and Dubinin–Radushkevich models were respectively 0.980, 0.930 and 0.968 for ZnO:Pb 2% and 0.994, 0.982 and 0.818 for ZnO:Pb 4%. A high value of R^2 was obtained by the Langmuir model. Also the R_L constant of the Langmuir isotherm for ZnO:Pb 2% and ZnO:Pb 4%, for different concentrations of RB5 (20–80 mg/L), was between 0 and 1, which indicates the favorable adsorption of RB5 onto ZnO:Pb NPs under the

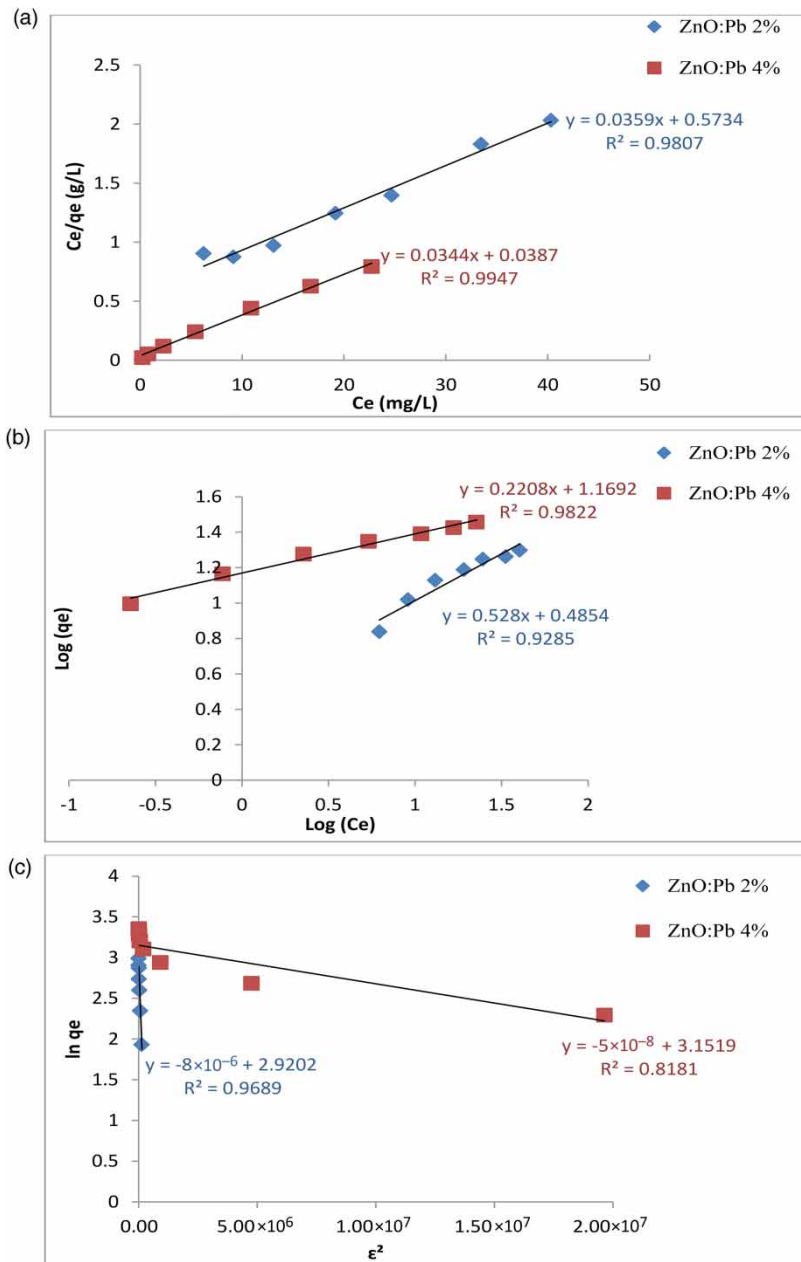


Figure 8 | Langmuir (a), Freundlich (b) and Dubinin–Radushkevich (c) isotherms for RB5 dye adsorption onto ZnO:Pb NPs.

conditions used in this study. The result shows that the Langmuir isotherm model provided a good fit to the sorption equilibrium data. A similar isotherm model was observed in the adsorption of RB5 on modified dolomite (Ziane *et al.* 2018). The maximum monolayer adsorption capacities of ZnO:Pb 2% and ZnO:Pb 4% are respectively 27.85 mg/g and 29.1 mg/g, which are higher than results found using only ZnO for adsorption of RB5 (3.64 mg/g) (Saeed 2013).

A comparison of maximum adsorption capacity on ZnO:Pb (2 and 4%) NPs with other adsorbents for RB5 dye removal is listed in Table 8. The ZnO:Pb adsorbent has relatively higher maximum adsorption capacity toward RB5 dye than most of the listed adsorbents.

The isotherm models describe how the adsorbent interacts with the adsorbate. Figure 9 presents the experimental isotherms of sorption of RB5 onto ZnO:Pb 2% and ZnO:Pb 4%. The sorption of RB5 onto the NPs ZnO:Pb 2%

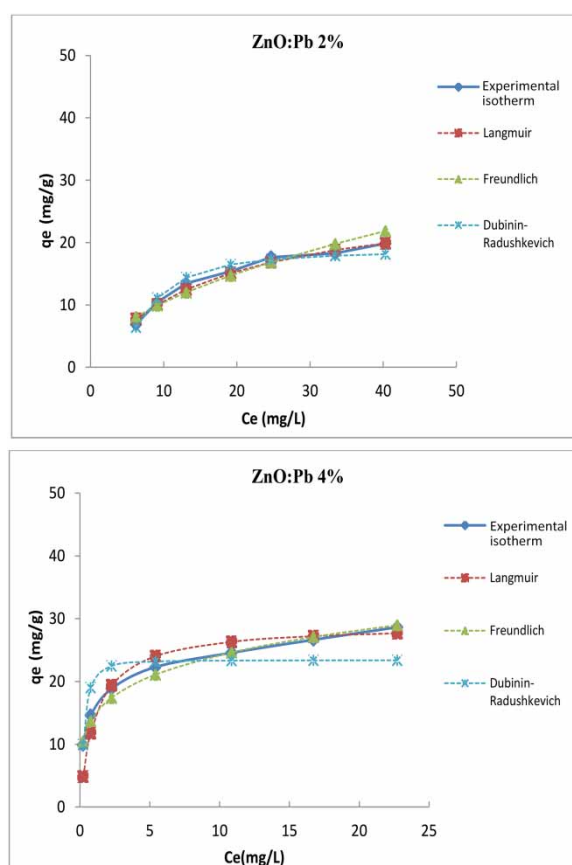
Table 7 | Isotherm constant parameters and correlation coefficient calculated for the sorption of RB5 onto ZnO:Pb 2 and 4%

Isotherm	Plot	Parameters	Value of parameters	
			ZnO:Pb 2%	ZnO:Pb 4%
Langmuir	C_e/q_e vs C_e	K_L (L/mg)	0.062	0.88
		q_m (mg/g)	27.85	29.06
		R_L	0.72–0.29	0.99–0.42
		R^2	0.980	0.994
Freundlich	Log q_e vs log C_e	K_f (mg ^{1-(1/n)} /L ^(1/n) /g)	3.06	14.52
		1/n	0.53	0.22
		R^2	0.930	0.982
Dubinin–Radushkevich	Ln q_e vs ε^2	K (mol ² /J ²)	-8.10^{-6}	-5.10^{-8}
		q_s (mg/g)	18.67	23.38
		R^2	0.968	0.818

Table 8 | RB5 sorption capacity by different adsorbents

Adsorbents	Maximum sorption capacity (mg/g)	References
High lime fly ash	7.9	Eren & Acar (2007)
Cetyltrimethyl ammonium bromide modified zeolite	12.9	Karadag <i>et al.</i> (2007)
Peat	7	Ip <i>et al.</i> (2009)
ZnO	3.6	Saeed (2013)
ZnO-Fe ₃ O ₄	22.1	Farrokhi <i>et al.</i> (2014)
TiO ₂ -NPs	88.5	Shaheed & Hussein (2014)
Multiwall carbon nanotubes	36.2	Samadi <i>et al.</i> (2015)
Mn ₂ O ₃	14.6	Nassar <i>et al.</i> (2016)
Iron oxide NPs	18	Chang & Shih (2018)
ZnO:Pb 2%	27.85	Present study
ZnO:Pb 4%	29.1	Present study

and ZnO:Pb 4% were Class Langmuir (L); this class proposes, at low concentration in solution, a downward concavity which reflects a decrease in free sites as the adsorption progresses. This phenomenon occurs when the attractive forces between the adsorbed molecules are low. It is often observed when the molecules are adsorbed flat, which minimizes their lateral attraction. It can also appear when the molecules are adsorbed vertically and when the adsorption competition between the solvent and the solute is weak (Foo & Hameed 2010).

**Figure 9** | Comparison of isotherm models with experimental data (pH = 7, contact time = 24 h, T = 20 ± 2 °C and [RB5] = (20–80 mg/L)).

CONCLUSION

Pb doped ZnO showed a good efficiency in the sorption of the synthetic textile dye RB5. The influence of experimental parameters on RB5 removal percentage was investigated by

an experimental design methodology allowing the optimization of pH, NPs dose and contact time. The maximum color removal was 79.4% for ZnO:Pb 2% and 98.1% for ZnO:Pb 4% obtained at pH 7 for dose of NPs of 2 g/L and 79 min as contact time. The equilibrium and kinetic studies were investigated and the results show that the pseudo-second-order model presented excellent fit of the adsorption data. The Langmuir monolayer model was found to best fit the isotherm data. The maximum adsorption capacities of ZnO:Pb 2% and ZnO:Pb 4%, according to the Langmuir isotherm model, were 27.85 and 29.1 mg/g respectively. The kinetic and isotherm sorption parameters were compared to other published studies and the magnitude of their values highlights the benefits of ZnO:Pb NPs for textile effluent treatment.

ACKNOWLEDGEMENTS

We thank Water Research and Technologies Center, Borj Cedria-Tunisia, European Membrane Institute Montpellier-France and Faculty of Sciences of Gabes-Tunisia for financial support of this work.

CONFLICT OF INTEREST

On behalf of all authors, the corresponding author states that there is no conflict of interest.

DATA AVAILABILITY STATEMENT

All relevant data are included in the paper or its Supplementary Information.

REFERENCES

- Bazrafshan, E., Kord Mostafapour, F., Rahdar, S. & Mahvi, A. H. 2015 Equilibrium and thermodynamics studies for decolorization of Reactive Black 5 (RB5) by adsorption onto MWCNTs. *Desalination and Water Treatment* **54** (8), 2241–2251. <https://doi.org/10.1080/19443994.2014.895778>
- Bordbar, M., Sayban, Z., Yeganeh-Faal, A. & Khodadadi, B. 2018 Incorporation of Pb²⁺, Fe²⁺ and Cd²⁺ ions in ZnO nanocatalyst for photocatalytic activity. *Iranian Journal of Catalysis* **8** (2), 113–120.
- Borhade, A. V., Uphade, B. K. & Tope, D. R. 2013 PbO as an efficient and reusable catalyst for one-pot synthesis of tetrahydro benzo pyrans and benzylidene malonitriles. *Journal of Chemical Sciences* **125** (3), 583–589. <https://doi.org/10.1007/s12039-013-0396-8>.
- Chang, M. & Shih, Y. H. 2018 Synthesis and application of magnetic iron oxide nanoparticles on the removal of Reactive Black 5: reaction mechanism, temperature and pH effects. *Journal of Environmental Management* **224**, 235–242. <https://doi.org/10.1016/j.jenvman.2018.07.021>.
- Crini, G. & Lichtfouse, E. 2019 Advantages and disadvantages of techniques used for wastewater treatment. *Environmental Chemistry Letters* **17** (1), 145–155. doi:10.1007/s10311-018-0785-9.
- Dassi, R. B., Chamam, B. & Trabelsi, I. 2017 Combination of coagulation-flocculation and adsorption on granular activated carbon for color removal from AR18 and real textile wastewater. *Journal of the Tunisian Chemical Society* **19**, 295–302.
- Dil, E. A., Ghaedi, M., Asfaram, A., Mehrabi, F. & Sadeghfard, F. 2019 Efficient adsorption of Azure B onto CNTs/Zn:ZnO@Ni₂P-NCs from aqueous solution in the presence of ultrasound wave based on multivariate optimization. *Journal of Industrial and Engineering Chemistry* **74**, 55–62. <https://doi.org/10.1016/j.jiec.2018.12.050>.
- Dubinín, M. M. 1947 *The Equation of the Characteristic Curve of Activated Charcoal*. In: Dokl. Akad. Nauk, pp. 327–329.
- Ebrahimi, R., Hossienzadeh, K., Maleki, A., Ghanbari, R., Rezaee, R., Safari, M. & Puttaiah, S. H. 2019 Effects of doping zinc oxide nanoparticles with transition metals (Ag, Cu, Mn) on photocatalytic degradation of Direct Blue 15 dye under UV and visible light irradiation. *Journal of Environmental Health Science and Engineering* **17** (1), 479–492. <https://doi.org/10.1007/s40201-019-00366-x>.
- El Mir, L., El Ghouli, J., Alaya, S., Salem, M. B., Barthou, C. & Von Bardeleben, H. J. 2008 Synthesis and luminescence properties of vanadium-doped nanosized zinc oxide aerogel. *Physica B: Condensed Matter* **403** (10–11), 1770–1774. <https://doi.org/10.1016/j.physb.2007.10.069>.
- Eren, Z. & Acar, F. N. 2007 Equilibrium and kinetic mechanism for Reactive Black 5 sorption onto high lime Soma fly ash. *Journal of Hazardous Materials* **143** (1–2), 226–232. <https://doi.org/10.1016/j.jhazmat.2006.09.017>.
- Farrokhi, M., Hosseini, S. C., Yang, J. K. & Shirzad-Siboni, M. 2014 Application of ZnO–Fe₃O₄ nanocomposite on the removal of azo dye from aqueous solutions: kinetics and equilibrium studies. *Water, Air, & Soil Pollution* **225** (9), 2113. <https://doi.org/10.1007/s11270-014-2113-8>.
- Foo, K. Y. & Hameed, B. H. 2010 Insights into the modeling of adsorption isotherm systems. *Chemical Engineering Journal* **156** (1), 2–10. doi:10.1016/j.cej.2009.09.013.
- Freundlich, H. 1906 Over the adsorption in solution. *The Journal of Physical Chemistry* **57**, 385–470.
- Gehrke, I., Geiser, A. & Somborn-Schulz, A. 2015 Innovations in nanotechnology for water treatment. *Nanotechnology, Science and Applications* **8**, 1. <https://doi.org/10.2147/NSA.S43773>.
- Ghaedi, M., Khafri, H. Z., Asfaram, A. & Goudarzi, A. 2016 Response surface methodology approach for optimization of adsorption of Janus Green B from aqueous solution onto

- ZnO/Zn(OH)₂-NP-AC: kinetic and isotherm study. *Spectrochimica Acta Part A: Molecular and Biomolecular Spectroscopy* **152**, 233–240. <https://doi.org/10.1016/j.saa.2015.06.128>.
- Gita, S., Hussan, A. & Choudhury, T. G. 2017 Impact of textile dyes waste on aquatic environments and its treatment. *Environment & Ecology* **35** (3C), 2349–2353.
- Heibati, B., Rodriguez-Couto, S., Amrane, A., Rafatullah, M., Hawari, A. & Al-Ghouti, M. A. 2014 Uptake of Reactive Black 5 by pumice and walnut activated carbon: chemistry and adsorption mechanisms. *Journal of Industrial and Engineering Chemistry* **20** (5), 2939–2947. <https://doi.org/10.1016/j.jiec.2013.10.063>.
- Holkar, C. R., Jadhav, A. J., Pinjari, D. V., Mahamuni, N. M. & Pandit, A. B. 2016 A critical review on textile wastewater treatments: possible approaches. *Journal of Environmental Management* **182**, 351–366. <https://doi.org/10.1016/j.jenvman.2016.07.090>.
- Ip, A. W. M., Barford, J. P. & McKay, G. 2009 Reactive Black dye adsorption/desorption onto different adsorbents: effect of salt, surface chemistry, pore size and surface area. *Journal of Colloid and Interface Science* **337** (1), 32–38. <https://doi.org/10.1016/j.jcis.2009.05.015>.
- Karadag, D., Turan, M., Akgul, E., Tok, S. & Faki, A. 2007 Adsorption equilibrium and kinetics of Reactive Black 5 and reactive red 239 in aqueous solution onto surfactant-modified zeolite. *Journal of Chemical & Engineering Data* **52** (5), 1615–1620. <https://doi.org/10.1021/jc7000057>.
- Kataria, N. & Garg, V. K. 2017 Removal of Congo red and Brilliant green dyes from aqueous solution using flower shaped ZnO nanoparticles. *Journal of Environmental Chemical Engineering* **5** (6), 5420–5428. <https://doi.org/10.1016/j.jece.2017.10.035>.
- Khezami, L., Taha, K. K., Ghiloufi, I. & El Mir, L. 2016 Adsorption and photocatalytic degradation of malachite green by vanadium doped zinc oxide nanoparticles. *Water Science and Technology* **73** (4), 881–889. <https://doi.org/10.2166/wst.2015.555>.
- Khezami, L., Taha, K. K. & Modwi, A. 2017a Efficient removal of cobalt from aqueous solution by zinc oxide nanoparticles: kinetic and thermodynamic studies. *Zeitschrift für Naturforschung A* **72** (5), 409–418. <https://doi.org/10.1515/zna-2016-0477>.
- Khezami, L., Taha, K. K., OuldM'hamed, M. & Lemine, O. M. 2017b (x)ZnO(1 – x)Fe₂O₃ nanocrystallines for the removal of cadmium(II) and nickel(II) from water: kinetic and adsorption studies. *Journal of Water Supply: Research and Technology – AQUA* **66** (6), 381–391. <https://doi.org/10.5004/dwt.2016.0196>.
- Kulkarni, S. D., Kumbar, S., Menon, S. G., Choudhari, K. S. & Santhosh, C. 2016 Magnetically separable core-shell ZnFe₂O₄@ZnO nanoparticles for visible light photodegradation of methyl orange. *Materials Research Bulletin* **77**, 70–77. <https://doi.org/10.1016/j.materresbull.2016.01.022>.
- Kumar, K. Y., Muralidhara, H. B., Nayaka, Y. A., Balasubramanyam, J. & Hanumanthappa, H. 2013 Low-cost synthesis of metal oxide nanoparticles and their application in adsorption of commercial dye and heavy metal ion in aqueous solution. *Powder Technology* **246**, 125–136. <https://doi.org/10.1016/j.powtec.2013.05.017>.
- Langmuir, I. 1916 The constitution and fundamental properties of solids and liquids. Part I solids. *Journal of the American Chemical Society* **38**, 2221–2295.
- Lei, C., Pi, M., Xu, D., Jiang, C. & Cheng, B. 2017 Fabrication of hierarchical porous ZnO-Al₂O₃ microspheres with enhanced adsorption performance. *Applied Surface Science* **426**, 360–368. <https://doi.org/10.1016/j.apsusc.2017.07.095>.
- Maleki, A., Mohammad, M., Emdadi, Z., Asim, N., Azizi, M. & Safaei, J. 2018 Adsorbent materials based on a geopolymer paste for dye removal from aqueous solutions. *Arabian Journal of Chemistry*. <https://doi.org/10.1016/j.arabjc.2018.08.011>
- Montazer-Rahmati, M. M., Rabbani, P., Abdolali, A. & Keshtkar, A. R. 2011 Kinetics and equilibrium studies on biosorption of cadmium, lead, and nickel ions from aqueous solutions by intact and chemically modified brown algae. *Journal of Hazardous Materials* **185** (1), 401–407. <https://doi.org/10.1016/j.jhazmat.2010.09.047>.
- Nonvisade, P. & Siriphannon, P. 2009 Chitosan intercalated montmorillonite: preparation, characterization and cationic dye adsorption. *Applied Clay Science* **42** (3–4), 427–431. <https://doi.org/10.1016/j.clay.2008.04.013>.
- Mousavi, S. M., Mahjoub, A. R. & Abazari, R. 2015 Green synthesis of ZnO hollow sphere nanostructures by a facile route at room temperature with efficient photocatalytic dye degradation properties. *RSC Advances* **5** (130), 107378–107388. <https://doi.org/10.1039/C5RA19507A>.
- Mustafa, G., Tahir, H., Sultan, M. & Akhtar, N. 2013 Synthesis and characterization of cupric oxide (CuO) nanoparticles and their application for the removal of dyes. *African Journal of Biotechnology* **12** (47), 6650–6660. <http://dx.doi.org/10.5897/AJB2013.13058>.
- Nassar, M. Y., Amin, A. S., Ahmed, I. S. & Abdallah, S. 2016 Sphere-like Mn₂O₃ nanoparticles: facile hydrothermal synthesis and adsorption properties. *Journal of the Taiwan Institute of Chemical Engineers* **64**, 79–88. <https://doi.org/10.1016/j.jtice.2016.03.041>.
- Qu, X., Alvarez, P. J. & Li, Q. 2013 Applications of nanotechnology in water and wastewater treatment. *Water Research* **47** (12), 3931–3946. <http://dx.doi.org/10.1016/j.watres.2012.09.058>.
- Riera-Torres, M., Gutiérrez-Bouzán, C. & Crespi, M. 2010 Combination of coagulation–flocculation and nanofiltration techniques for dye removal and water reuse in textile effluents. *Desalination* **252** (1–3), 53–59. <https://doi.org/10.1016/j.desal.2009.11.002>.
- Saeed, W. N. M. 2013 Removal of azo dye Reactive Black 5 by adsorption onto ZnO and CaO. *Journal of Kerbala University* **11** (4), 321–330. <https://doi.org/10.1080/19445994.2013.811114>.
- Salehi, K., Shahmoradi, B., Bahmani, A., Pirsaeheb, M. & Shivaraju, H. 2016 Optimization of Reactive Black 5 degradation using hydrothermally synthesized NiO/TiO₂ nanocomposite under natural sunlight irradiation.

- Desalination and Water Treatment* **57** (52), 25256–25266. <https://doi.org/10.1080/19443994.2016.1149890>.
- Samadi, M. T., Zolghadrmasab, H., Godini, K., Poormohammadi, A., Ahmadian, M. & Shanesaz, S. 2015 Kinetic and adsorption studies of Reactive Black 5 removal using multi-walled carbon nanotubes from aqueous solution. *Der Pharma Chemica* **7** (5), 267–274.
- Santhosh, C., Velmurugan, V., Jacob, G., Jeong, S. K., Grace, A. N. & Bhatnagar, A. 2016 Role of nanomaterials in water treatment applications: a review. *Chemical Engineering Journal* **306**, 1116–1137. <https://doi.org/10.1016/j.cej.2016.08.053>.
- Sathya, M. & Pushpanathan, K. 2018 Synthesis and optical properties of Pb doped ZnO nanoparticles. *Applied Surface Science* **449**, 346–357. <https://doi.org/10.1016/j.apsusc.2017.11.127>.
- Shaheed, M. A. & Hussein, F. H. 2014 Adsorption of Reactive Black 5 on synthesized titanium dioxide nanoparticles: equilibrium isotherm and kinetic studies. *Journal of Nanomaterials* **2014**. <https://doi.org/10.1155/2014/198561>.
- Singh, K. P., Mohan, D., Sinha, S., Tondon, G. S. & Gosh, D. 2003 Color removal from wastewater using low-cost activated carbon derived from agricultural waste material. *Industrial & Engineering Chemistry Research* **42** (9), 1965–1976. <https://doi.org/10.1021/ie020800d>.
- Verma, A. K., Bhunia, P. & Dash, R. R. 2012 Supremacy of magnesium chloride for decolourisation of textile wastewater: a comparative study on the use of different coagulants. *International Journal of Environmental Science and Development* **3** (2), 118. <https://doi.org/10.7763/IJESD.2012.V3.200>.
- Wong, C. P. P., Lai, C. W., Lee, K. M. & Hamid, S. B. A. 2015 Advanced chemical reduction of reduced graphene oxide and its photocatalytic activity in degrading Reactive Black 5. *Materials* **8** (10), 7118–7128. <https://doi.org/10.3390/ma8105363>.
- Zhang, F., Chen, X., Wu, F. & Ji, Y. 2016 High adsorption capability and selectivity of ZnO nanoparticles for dye removal. *Colloids and Surfaces A: Physicochemical and Engineering Aspects* **509**, 474–483. <https://doi.org/10.1016/j.colsurfa.2016.09.059>.
- Ziane, S., Bessaha, F., Marouf-Khelifa, K. & Khelifa, A. 2018 Single and binary adsorption of Reactive Black 5 and Congo red on modified dolomite: performance and mechanism. *Journal of Molecular Liquids* **249**, 1245–1253. <https://doi.org/10.1016/j.molliq.2017.11.130>.

First received 12 July 2020; accepted in revised form 1 October 2020. Available online 17 October 2020